Biofabrication

PAPER

A gel aspiration-ejection system for the controlled production and delivery of injectable dense collagen scaffolds

RECEIVED
8 May 2015

REVISED
26 January 2016

ACCEPTED FOR PUBLICATION
12 February 2016

PUBLISHED
22 March 2016

Neysan O Kamranpour, Amir K Miri, Mark James-Bhasin and Showan N Nazhat

Department of Mining and Materials Engineering, McGill University, Canada

E-mail: showan.nazhat@mcgill.ca

Keywords: extracelullar matrix, tissue equivalents, injectable, dense collagen gels, osteogenesis, hydraulic permeability, plastic compression

Supplementary material for this article is available online

Abstract

A gel aspiration-ejection (GAE) system has been developed for the advanced production and delivery of injectable dense collagen (I-DC) gels of unique collagen fibrillar densities (CFDs). Through the creation of negative pressure, GAE aspirates prefabricated highly hydrated collagen gels into a needle, simultaneously inducing compaction and meso-scale anisotropy (i.e., fibrillar alignment) on the gels, and by subsequent reversal of the pressure, I-DC gels can be controllably ejected. The system generates I-DC gels with CFDs ranging from 5 to 32 wt%, controlling the initial scaffold microstructure, anisotropy, hydraulic permeability, and mechanical properties. These features could potentially enable the minimally invasive delivery of more stable hydrogels. The viability, metabolic activity, and differentiation of seeded mesenchymal stem cells (MSCs) was investigated in the I-DC gels of distinct CFDs and extents of anisotropy produced through two different gauge needles. MSC osteoblastic differentiation was found to be relatively accelerated in I-DC gels that combined physiologically relevant CFDs and increased fibrillar alignment. The ability to not only support homogenous cell seeding, but also to direct and accelerate their differentiation through tissue-equivalent anisotropy, creates numerous opportunities in regenerative medicine.

1. Introduction

Tissue engineering and regenerative medicine aims to restore tissue function through delivery of viable elements and their host integration [1]. Because of their innate structural and compositional similarities to the native extracellular matrix (ECM) and their extensive framework for cellular proliferation and survival, hydrogels can be used to locally and controllably deliver therapeutics [2]. Hydrogels can also be injectable, thereby reducing the invasiveness, time, cost, and complexity of surgical procedures and accelerating postoperative healing. As the most abundant ECM protein in connective tissues and bone, fibrillar type-I collagen provides the key scaffolding material in the human body, dictating tissue mechanical properties, while signaling back to maintain a differentiated cell phenotype. In this regard, extracted, acid solubilized type-I collagen molecules, which self-assemble at physiological pH and temperature, are attractive as injectable hydrogels [3]. However, the currently available highly hydrated collagen (HHC)-based gels rely on postinjection geling, which forms hydrogels of randomly entangled nanofibrillar frameworks [3] that exert no microstructural control and do not fully mimic the highly organized components of native ECM and bone structures. In addition, as a consequence of their low collagen fibrillar density (CFD; $<$1 wt%), these hydrogels have weak mechanical properties, undergo significant cell-mediated contraction [4, 5], and are rapidly resorbed *in vivo* [6]. While chemical crosslinking increases the durability of HHC gels [7], it negatively impacts their biocompatibility [8, 9]. In effect, currently available injectable collagen hydrogels lack physiological relevance.

Among the techniques to increase gel CFD [10–14], plastic compression (PC) has been shown to be a rapid, cell-independent process that generates cell seeded, mechanically strong, dense collagen (DC; $>$5 wt% CFD) gels [13]. These osteoid mimicking DC gels have supported the osteogenic differentiation of three-dimensional seeded preosteoblasts and

mesenchymal stem cells (MSCs) *in vitro* [15–18]. However, while DC gels are of physiologically relevant CFDs, these matrices retain the initial random nanofibrillar arrangement and lack the preferred structured organization of native tissues, yielding a nondirectional permeability field. Moreover, these DC gels are not injectable, which ultimately limits their potential clinical applicability.

Recently, collagen gel aspiration-ejection (GAE) was introduced as a technique to produce injectable dense collagen (I-DC) gels with tuneable CFDs and microstructures [19]. Through the creation of negative pressure, GAE initially aspirates prefabricated HHC gels into a blunt needle of a predefined lumen size, simultaneously imparting compaction and meso-scale anisotropy on the gels, and by subsequent reversal of the pressure, I-DC gels can be controllably ejected. I-DC gels have demonstrated significant collagen fibril alignment, impacting seeded MSC morphology and differentiation [19]. In order to advance the GAE technique, this study reports on the development of a system for the production and delivery of I-DC gels. The effect of needle lumen size on initial I-DC CFDs as produced through gauge numbers 8G through 14G, as well as their tensile mechanical properties, and extent of directionality (alignment) was investigated. In addition, the ability of I-DC gels in regulating anisotropic permeability was established through a mathematical model. Furthermore, the impact of gel CFD and extent of alignment on seeded MSC proliferation and osteoblastic differentiation was investigated in I-DC gels produced through two needle gauge numbers and compared to those seeded in PC produced DC gels.

2. Materials and methods

2.1. Processing of HHC gels

Precursor HHC gels were processed by neutralizing a 4:1 ratio of 6.0 mg ml^{-1} in 0.6% acidic solution (Collagen Solutions LTD, UK) of sterile bovine dermis derived type-I collagen and 10X concentrated Dulbecco's Modified Eagle Medium (10X DMEM; Sigma Aldrich, Canada) with 480 μl of 5N NaOH [20]. The neutralized solution was then cast in 1.5 ml aliquots into the cylindrical molds of a 48-well plate (Corning Costar, USA) and incubated at 37 °C for 30 min to complete gelation.

2.2. I-DC gel production through GAE

As cast, precursor HHC cylindrical gels were processed into I-DC gels through a GAE system (figure 1(a)) comprised of an angioplasty inflation device (AID; B Braun, Germany) to apply pressure differentials attached to a fluid transfer syringe (Fisher), which introduced an incompressible fluid, necessary for gel ejection, into the chamber of the AID. The connection between the AID and syringe was achieved via two Luer lock valves attached in series to control flow direction. An interchangeable needle (Hamilton Co., USA) was then attached to the port of the most distal Luer lock valve.

The GAE process was initiated by completely inserting the piston of AID into its cylinder component followed by gently positioning the attached needle at the concentric surface center of the HHC gel. Aspiration was applied by gently retracting the piston to generate negative pressure (~0.01–1 bar) and draw the HHC gel into the needle. Once the gel was almost fully drawn into the needle, the vacuum line was closed by locking the distal Luer lock valve. This step prevented the I-DC gel from entering the cylindrical chamber of AID. At this point, the compacted hydrogel remained in position within the needle tip and ready for ejection.

To ensure controlled ejection of the I-DC gels, the syringe was filled with a sterile incompressible fluid (e.g., water, phosphate buffered saline, culture media) and introduced through the proximal Luer lock valve with an open setting between the syringe and AID. The two Luer lock valves were then adjusted manually to open the pathway directly between the densification needle and AID. Next, positive pressure was applied through AID to controllably eject the I-DC gel. Through the GAE system, the properties of I-DC gels produced using needle gauge numbers 8G, 10G, 12G, and 14G were investigated. Depending on the length and diameter of the gel, which were dictated by the dimensions of the precursor HHC gel and the needle gauge number, the required aspiration pressure and time varied from ~0.05 bar and ~10 s, respectively, for 8G needles to ~1 bar and ~100 s for 14G needles.

2.3. DC gel production through PC

DC gels were produced by the PC method, as previously described [13]. Briefly, precursor HHC gels were placed between two nylon meshes and on top of a steel mesh and absorbent pad. DC gels were produced by applying a 1 kPa compressive stress for 5 min.

2.4. Determination of gel CFD

Previously reported CFD values were used [19, 20]. In brief, the weight percent of collagen in the precursor HHC gels and after GAE or PC was calculated by weighing the gels (n = 5) before and after freeze drying (BenchTop K, VirTis, Canada).

2.5. Mechanical analysis of I-DC gels

Tensile testing was carried out on I-DC gels produced through GAE using needle gauge numbers 8G, 10G, 12G, and 14G. The I-DC gel specimens (n = 5) with 5 mm gauge length were mounted onto a silicon carbide paper interface with cyanoacrylate glue to facilitate their attachment to the grippers of an ElectroForce Biodynamic 5160 tensile test instrument (Bose Corp., USA). Tensile tests were carried out using a 20 N load cell and a controlled displacement rate of

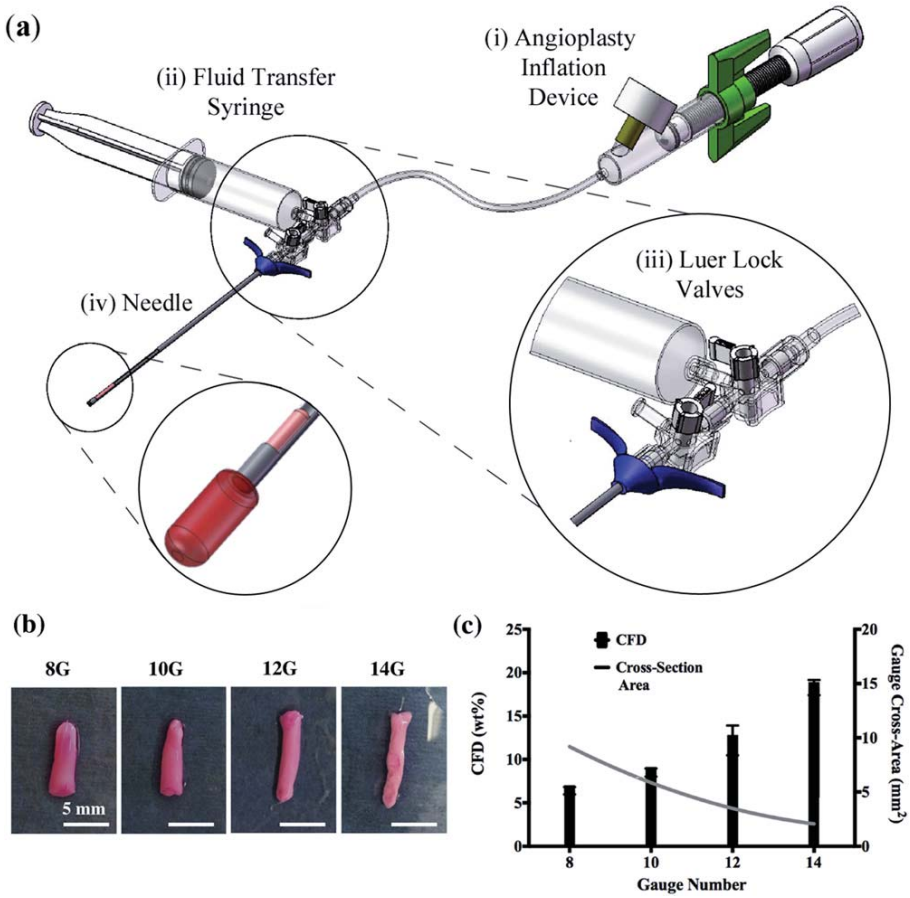

Figure 1. Standardized GAE for I-DC gel production and CFD characterization. (a) GAE system consisting of (*i*) AID, (*ii*) fluid transfer syringe, (*iii*) two Luer lock valves, and (*iv*) densification needle. Expanded figures showing Luer lock valve configuration and precursor HHC gel during I-DC processing. (b) Images of ejected I-DC gels from 8G, 10G, 12G, and 14G needles. (c) I-DC gel CFDs (black bars) versus needle gauge number and cross-sectional area (grey line).

0.01 mm s^{-1}. Specimens were kept hydrated with droplets of deionized water. The initial load versus displacement data was processed to generate a corresponding stress–strain curve by using the needle internal diameter (3.43, 2.69, 2.16, and 1.60 mm corresponding to 8G, 10G, 12G, and 14G, respectively) as the nominal gauge diameter of each I-DC gel specimen and initial gauge length for stress and strain calculations, respectively. The apparent modulus and UTS were calculated from the linear region of the stress–strain curves and maximum stress values, respectively.

2.6. Microstructural analysis

Scanning electron microscopy (SEM) and nonlinear laser scanning microscopy (NLSM) imaging, based on second-harmonic generation, were used to investigate the microstructures of I-DC gels and compared to those DC gels produced through PC, as well as demineralized bone (DMBB) and tendon samples. Demineralized bone samples were prepared from bovine femur and cut into longitudinal and horizontal sections before fixing in 10% methanol free formaldehyde for 72 h and placed in a 5 M formic acid solution for a 5-week demineralization period [21]. Longitudinally cut tendon biopsies were dissected from rat tails preserved in 4% formaldehyde. The tissue samples were then rinsed in deionized water and prepared for either SEM or NLSM imaging as described below.

For SEM analysis, the I-DC and DC gels were initially fixed in 4% formaldehyde for 30 min followed by rinsing in deionized distilled water for 15 min. Subsequently, all samples were dehydrated through a graded series of ethanol solutions, followed by chemical drying using 1,1,1,3,3,3-hexamethyldisilazane (Fischer). SEM analysis was performed on 25 s Au Pd^{-1} sputter coated samples (Hummer VI Sputter Coater, Ladd Research Industries) with a Field Emission-STEM (FEI-50; SEM Fei Inspect FEI, The Netherlands) at 5 kV and 10 mA with a working distance of 10 mm.

For NLSM analysis, the I-DC and DC gels were initially fixed in 4% formaldehyde for 30 min followed by rinsing in deionized distilled water for 15 min. Subsequently, all samples were placed in a 70% ethanol solution overnight before paraffin mounting in blocks, then sectioned into 60 μm thick specimens and placed onto glass slides. A Lecia Microsystems

(Germany) multiphoton microscope was used for confocal imaging with two-photon excitation to visualize collagen fibrillar alignment and orientation. An 830 nm wavelength pulsing laser with nearly 20–30 mW output power with tuning range between 680–1080 was used as the excitation source. The light emission of the collagen under excitation was imaged through a collection objective of 63X oil immersion lens (Lecia) and a 2 mm working distance. The sample stage was manually moved along the x-y-z planes through a control unit with electric motor actuators. 1264×1264 pixel digital images from a $100 \times 100\ \mu$m laser beam scanning area were captured in an 8-bit TIF image file format. Five central regions were surveyed across the 60 μm thick specimen sections and analyzed quantitatively to establish fibril orientation and dispersion angle. The central imaging areas were chosen to display the natural configuration of collagen fibrils.

NLSM generated images were analyzed for fibril directionality through ImageJ (NIH, USA) with the Fiji open-source plug-in [22]. The analysis was carried out using the directionality analysis tool within the applet and selecting the 'local gradient orientation' algorithm. The analysis provided a histogram with a dominant Gaussian distribution of fiber directionality, along with its dispersion angle, corresponding data population (between 0 and 1), and regression correlation coefficient (between 0 and 1). The data population represented the relative number of fibrils with the associated dispersion. The numerical results were used in the analysis for data populations higher than 0.70 and correlation coefficients higher than 0.90.

2.7. Culturing of seeded MSCs in I-DC gels

Passage 9 *Mus musculus* C57BL/6 bone marrow derived MSCs (Life technologies; Gibco) were incubated at 5% CO_2 and grown to 70% confluency at 37 °C. The expansion and growth medium consisted of DMEM/FK12 supplemented with 10% foetal bovine serum (FBS) and 5 μg ml^{-1} gentamicin antibiotic. Precursor HHC gels were processed by transferring 1.5 ml of neutralized bovine dermis derived collagen solution (6.00 mg ml^{-1}) seeded with MSCs at a density of 200 000 cells ml^{-1} into a 48-well plate and cast in an incubator with 5% CO_2 atmosphere at 37 °C for 30 min. MSC seeded I-DC gels produced through GAE using gauge numbers 8G and 12G were compared to those seeded in DC gels produced via PC. Culturing was carried out in 6-Well plates in either growth medium (nonosteogenic) or in osteogenic differentiation medium that consisted of α-MEM in place of DMEM/FK12 supplemented with 50 μM of β-glycerophosphate for up to day 21.

2.8. Cell metabolic activity and viability

The AlamarBlue™ assay (Life Technologies, Canada) was used to investigate the seeded MSC metabolic activity as an indicator of cell viability and proliferation [23]. Three biopsies of gels were stained in culture media with 10% AlamarBlue™ reagent and 10% FBS supplemented with 1% Penicillin-Streptomycin and incubated for 3 h under darkness in 5% CO_2 and 37 °C. A fluorescent detection system was employed using a TECAN 9600 epi-fluorescent plate reader with excitation at 535 and 600 nm for emission detection. Analysis was carried out at days 1, 11, 15, and 21 and plotted against the florescence intensity, which was proportional to the magnitude of metabolic activity.

Confocal laser scanning microscopy (CLSM; Carl Zeiss LSM510meta) was used to image seeded MSC viability and morphology at days 11 and 21 in culture. Gels were stained with 0.1 M calcein AM solution (i.e., in culture media) as a Live assay analysis and incubated at 37 °C for 15 min prior to viewing. Excitation and emission wavelengths of 490 and 530 nm were used to visualize the stained cells by plane scanning. The resulting emissions from the stain were detected for image assembly.

2.9. Cell gene expression

Quantitative polymerase chain reaction (q-PCR) was conducted to amplify alkaline phosphatase (*Alp*), Runt-related transcription factor 2 (*Runx2/Cbfa1*), and osteocalcin (*Ocn/Bglap*) transcripts as indicators of MSC osteogenic differentiation. Gels cultured in both nonosteogenic and osteogenic media were subjected to the PureLink® RNA kit (Life Technologies, Canada). This generated RNA transcripts that were reverse transcribed to cDNA by 200 U/μl M-MulV reverse transcriptase (NEB, USA) in a solution containing 10x reaction buffer, 2.5 mM of each deoxynucleotide triphosphate (NEB, USA), RNAse inhibitor at 10 U/μl, total RNA transcripts in water, and 50 μM oligo d(T). The reverse transcription reaction underwent incubation at 37 °C for 1 h and the temperature was increased to 50 °C upon completion to denature the reverse transcriptase. SYBR® Select (Life Technologies) q-PCR master mix and primer pairs: *Alp plus* 5′-*GGGAGATGGTATGGGCGTCT*-3′, *minus* 5′-*AGGGCCACAAAGGGGAATTT*-3′; *RunX2/Cbfa1 plus* 5′- *plus* 5′-*ATCCCCATCCATCCCTC*-3′, *minus* 5′-*CTGTCTGTGCCTTCTGGGTT*-3′; *Ocn/Bglap plus* 5′-*GACAAAGCCTTCATGTCCAAGC*-3′, *minus* 5′-*AGCAGGGTCAAGCTCACATAG*-3′; *Gapdh plus* 5′-*AAGGGCTCATGACCACAGTC*-3′, *minus* 5′-*CAGGGATGATGTTCTGGGCA*-3′ (200 nM each) were prepared for entry into the 7900HT q-PCR thermocycler (Applied Biosystems, USA). Cycling conditions were as follows: an initial denaturation of 95 °C for 10 min, followed by 40 repeats of 95 °C of denaturation for 15 s and an annealing/extension phase of 45 s. Using the delta–delta cycle threshold method, data was normalized to the expression of *Gapdh* and calibrated to the initial time point.

2.10. Statistical analysis

Fibril dispersion angles in I-DC gels were statistically compared to that in DC gel as well as DMBB and rat-tail tendon using ordinary one-way analysis of variance. Tukey's multiple comparisons test determined significant differences in MSC metabolic activities seeded in I-DC and DC gels. One-way analysis of variance was calculated using Bonferroni's multiple comparison test for significant differences. q-PCR data was statistically compared between gels cultured in nonosteogenic and osteogenic media. Additionally, the two populations of data sets were compared between the tested gels. Two-way analysis of variance was calculated, with a Bonferroni posttest correction to determine significant differences. A 95% confidence interval was used for each calculation.

3. Results and discussion

3.1. I-DC gel production with tuneable CFDs and mechanical properties

I-DC gels with tuneable CFDs and microstructures can be produced by GAE through the application of pressure differentials [19]. The GAE system developed in this study (figure 1(a)) reduced the variability of human subjectivity by applying controllable and adjustable aspirating and ejecting pressures via AID. In addition, the broader range of applicable pressures negated the use of absorbent paper in accelerating water expulsion and the compaction of precursor HHC gels (figure S1 shows the I-DC gels produced through the GAE process). By using needle gauge numbers 8G, 10G, 12G, and 14G in this GAE system (figure 1(b)), I-DC gels with distinct CFDs (figure 1(c)) and respective densification ratios (fold increase in CFD) of 7.5, 10.3, 14.8, and 22.3 were produced. The initial CFD value of the precursor HHC gels fibrilized from a collagen solution concentration of 6 mg ml^{-1} were approximately 0.8 wt%. Modifications of the initial collagen acidic-solution concentration in the precursor HHC and aspirating needle gauge number (i.e., diameter) yielded I-DC gels of CFDs in the range 5 ± 0.010 to 32 ± 0.026 wt% (figure S2(a)), demonstrating more control in producing I-DC gels of defined CFDs compared to the previously reported GAE method [19]. Furthermore, an increase in the ratio between the diameters of the precursor HHC (i.e., mold diameter) to the final I-DC gel size (i.e., needle diameter) led to an increase in I-DC CFD (figure S2(b)).

Quasistatic tensile testing indicated significant increases ($p < 0.05$) in apparent modulus and ultimate tensile strength (UTS) values with I-DC gel CFD (figures 2(a) and (b), respectively; figure S3 shows the representative stress-strain curves). As previously reported for rolled DC sheets [20, 24] produced by PC gel densification leads to an increase in contact points between collagen fibril bundles where greater frictional forces are accumulated, thus requiring greater levels of tensile stress.

3.2. I-DC gel microstructural characterisation

The microstructures of the I-DC gels of increasing CFDs were compared to those of DC as well as the samples derived from native DMBB and rat-tail tendon. Qualitatively, SEM micrographs (figure 3(a)) indicated localized microscale anisotropy in I-DC gels, which was attributable to bulk fibril orientation in the direction of gel aspiration, in contrast to DC gels, which showed collagen fibrils of random orientation [13]. SEM micrographs of DMBB and rat-tail tendon, taken parallel to the direction of growth, confirmed their highly ordered structures with clearly aligned collagenous fibrils.

NLSM allowed for the quantification of fibrillar orientation, as defined by direction and dispersion. Direction represented the mean orientation in a given volume of interest, whereas dispersion denoted the degree of deviation or scattering in the orientation of individual fibrils from the mean orientation. Thus, highly aligned collagen fibrils yielded smaller dispersion angles. Representative NLSM images showed typical fibril dispersion properties of I-DC gels of different CFDs aspirated through needle gauge numbers 8G, 10G, 12G, and 14G (figure 3(b)) and their post-processing (for randomly selected $100 \times 100\ \mu$m regions) using an ImageJ edge directionality algorithm determined their directionality histograms (figure 4(a)). A narrower normal Gaussian distribution of fiber directionality indicated an increase in fibrillar alignment, and there were significantly lower ($p < 0.05$) mean fibril dispersion angles (i.e., indices) in all I-DC gels compared to those in DC (figure 4(b)). Compared to PC, which compacts a gel in its entirety at the same time, thus providing little temporal and spatial dimension for fibrillar rearrangement, GAE compaction is more gradual and directional, initiating along one end of the precursor HHC and thus experiences the two-dimensional (i.e., planar) compaction process that provides the driving force for fibrillar rearrangement. However, the I-DC gels displayed significantly more dispersed collagen fibrils compared to both native derived tissues, which have a highly aligned collagenous microstructure that serve major functional roles [25–27]. While there were no significant differences in the mean fibril dispersion angles within the I-DC gels, those between 8G and 12G I-DC gels progressively decreased (along with their respective standard deviations), indicating greater extent of alignment, which then increased in that aspirated through the smaller 14G needle. This may be attributed to a gel compaction limit where shrinkage is no longer constrained to the expulsion of water, but also to the compaction and deformation of individual fibrils. Future studies will also investigate the extent of fibrillar alignment in regions at higher magnifications.

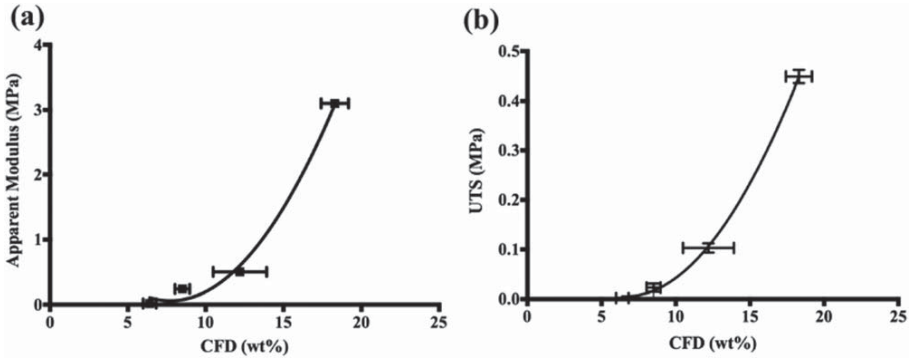

Figure 2. I-DC gel mechanical properties. (a) Apparent modulus and (b) and UTS as a function of I-DC gel CFD.

The progressive increase in alignment in I-DC gels produced through gauge numbers 8G, 10G, and 12G was reflected in their gross tensile stress–strain curve profiles (figure S3), which demonstrated a lack of the initial toe-region that is typical of randomly organized DC gels [13, 20, 24]. In contrast, the 14G I-DC gel demonstrated a clear toe-region, which is associated with fibrillar realignment in the direction of the applied stress [28, 29].

I-DC gels of similar CFDs produced using needle gauge numbers 8G, 10G, and 12G also displayed significantly ($p < 0.05$) lower collagen fibril dispersion compared to equivalent DC gels (figure S4).

3.3. Anisotropic I-DC gel permeability

The efficacy of the GAE system in regulating I-DC gel microstructure was assessed using bulk hydraulic permeability, a parameter dependent on the porosity, pore size, interconnectivity, and orientation of the fibrils [30]. Along with matrix stiffness [31] hydraulic permeability controls seeded cellular responses [17, 32], ultimately contributing to the biophysical properties of scaffolds through matrix remodeling [33]. Furthermore, knowledge of the bulk hydraulic permeability, representative of I-DC gel diffusive characteristics, may also allow for the utilization of I-DC gels as a controlled-release carrier of therapeutic agents in drug delivery systems. The biphasic nature of hydrogels provides an ideal microenvironment to control the release of bioactive molecules in drug delivery applications [34]. Although drug loading can be performed through covalent immobilization, predefined microstructures allow physical entrapments by simple encapsulation or affinity-based immobilization. In the latter case, the release profile may proceed through Darcy flow mechanisms [34], while involving transport processes. The transport capability of hydrogels can be represented by their bulk permeability [30]. To this end, a mathematical model was derived to simulate the permeability of I-DC gels (supplementary information) where the ratio of axial-to-radial permeability values was selected to demonstrate the role of needle gauge number.

An anisotropic I-DC gel may be regarded as a biphasic continuum with a porous solid phase, saturated by nonviscous freely moving fluid. It is assumed that the meso-scale, consisting of the fibrils, is one order of magnitude larger than the microscale, which consists of pores and fluid particles (figure 5(a)). The mathematical formulation used tensor notation to derive the permeability of a transversely isotropic I-DC gel structure. The tensor K denotes the effective (i.e., global) permeability tensor, where the ratio of longitudinal permeability (along the axial direction of the I-DC gels) to transverse permeability (along the thickness direction of the I-DC gels) was used to define the anisotropy. The anisotropy ratio (i.e., $K_x/K_{y,z}$) rapidly increased by transitioning from the DC to the I-DC gel, indicating the role of fibrillar alignment in regulating the diffusive properties of the porous structure (figure 5(b)). The gradient of variations was highest between the isotropic (DC) and anisotropic distributions of fibrillar orientation (e.g., I-DC 8G). The different needle gauge numbers regulated the ratio between the axial and radial permeabilities, potentially providing a tunable release profile for therapeutic delivery. The anisotropy ratio also depended on the CFD values, dramatically increasing in the case of tendon tissues.

3.4. Seeded MSC proliferation and differentiation in I-DC gels

It was previously demonstrated that the viability of seeded fibroblasts and MSCs was maintained in I-DC gels produced through GAE [19]. Furthermore, the GAE process imparted the immediate alignment of seeded cells along the fibrillar direction, ultimately accelerating their differentiation when compared to those seeded in DC gels. This study compared the effect of extent of fibrillar alignment in two I-DC gels of distinct CFDs on the proliferation and osteoblastic differentiation of seeded MSCs up to day 21 in nonosteogenic and osteogenic media. I-DC gels

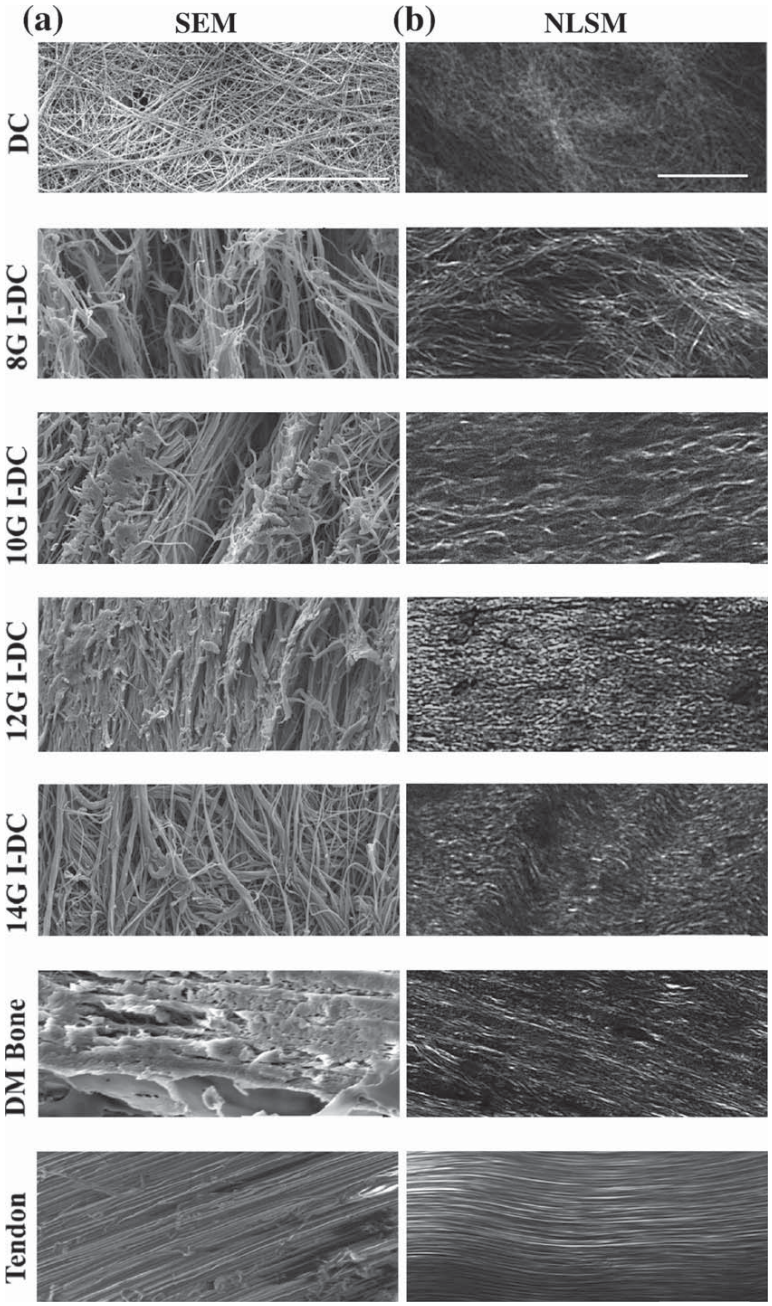

Figure 3. Microstructural analysis. (a) SEM micrographs and (b) NLSM images of I-DC gels produced by GAE through needle gauge numbers 8G (6 wt% CFD), 10G (8 wt% CFD), 12G (12 wt% CFD), and 14G (18 wt% CFD) and compared to DC (18 wt% CFD) produced through PC as well as demineralized bone and tendon samples (Scale bars = 10 and 25 μm, for SEM and NLAM images, respectively).

produced through 8G (6 wt% CFD) or 12G (12 wt% CFD), which were chosen since these provided either relatively large size or greater extent of fibrillar anisotropy, respectively. DC gels (18 wt% CFD) previously shown to promote the osteoblastic differentiation of seeded preosteoblasts and stem cells [15–18] were used as control.

Cell metabolic activity indicated that while there was an increase in proliferation up to day 15 in both media, significant ($p < 0.05$) divergence occurred beyond that time point, with MSCs cultured in non-osteogenic medium exhibiting greater metabolic activity when compared to those in osteogenic medium, which was attributable to the onset of cell differentiation [35, 36] (figure 6). In addition, in both media, there was significantly less ($p < 0.05$) metabolic activity in MSCs seeded in 12G I-DC when compared to those seeded in either 8G I-DC or DC gels, which may be attributed to either their relatively increased differentiation state or the smaller 12G I-DC

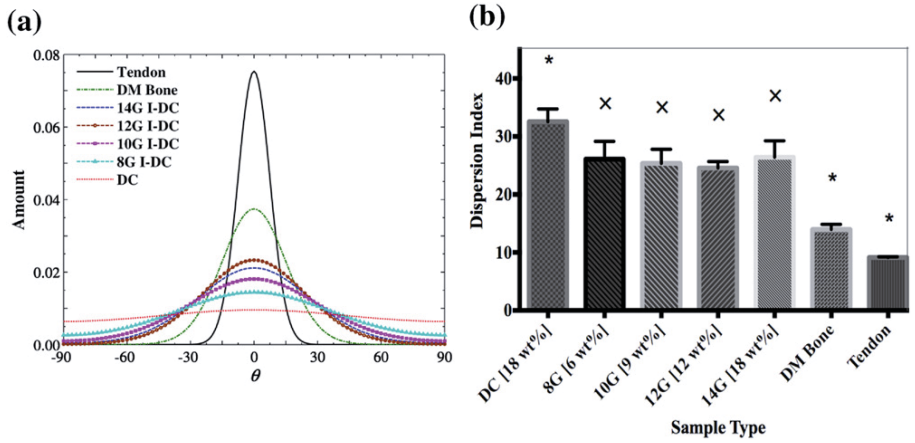

Figure 4. I-DC gel anisotropy. (a) Collagen fibril directionality calculated through NLSM image analysis (b) Mean collagen fibril dispersion angles generated from NLSM images. * indicates statistically significant ($p < 0.05$) differences. x indicates nonstatistically significant ($p > 0.05$) differences.

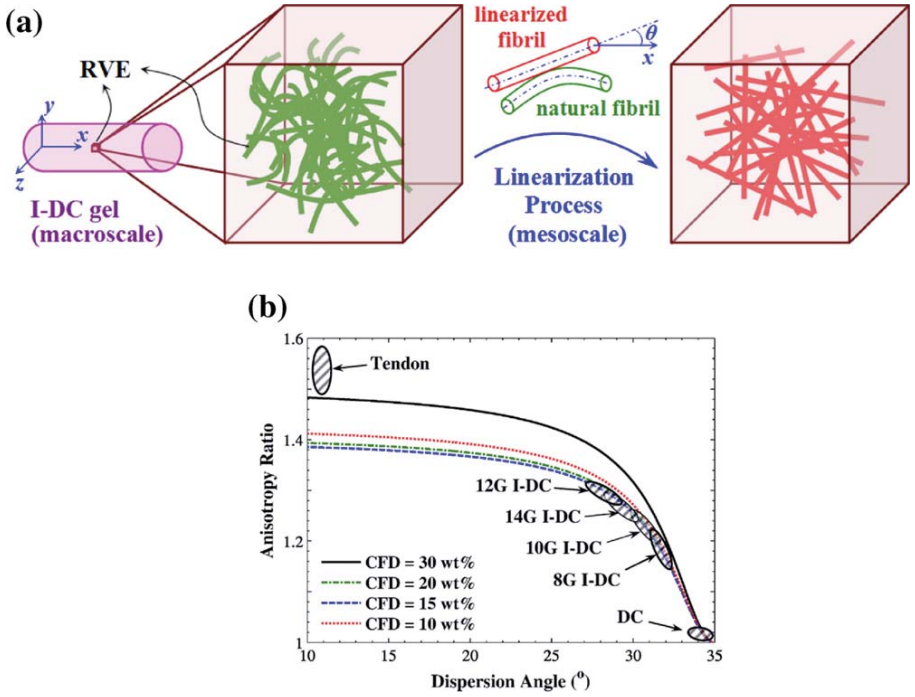

Figure 5. Modeling of I-DC gel permeability. (a) The problem geometry indicating a representative volume element (RVE) chosen from the I-DC gel and its linearization process. (b) Anisotropy ratio versus the dispersion angle, generated from equation (11) stacks.iop.org/BF/8/015018/mmedia, for a range of CFD values of DC, 8G I-DC, 12G I-DC, and tendon based on the NLSM data.

gel volume, which allowed less available space for proliferating cells to occupy. Along with an increase in gel CFD, the compaction process significantly increases seeded MSC density, which may control their proliferation through cell–cell contact inhibition [37].

CLSM images of Calcein AM stained seeded MSCs at day 11 demonstrated extensive viability in all gels. Furthermore, those cultured in 8G I-DC gel, and to a greater extent in those produced through 12G, were aligned preferentially along the longitudinal axis of the gels, confirming the ability of GAE to not only maintain the viability and proliferative capability of seeded cells, but also to effect their anisotropic alignment along the matrix (figure 7). In contrast, MSCs seeded in DC demonstrated no preferential orientation [38]. However, by day 21 in culture, cell alignment was less apparent in all gels attributable to extensive cell proliferation and matrix remodeling, thus occupying a large volume of the I-DC gels [37]. While cell-mediated matrix remodeling was not quantified in this

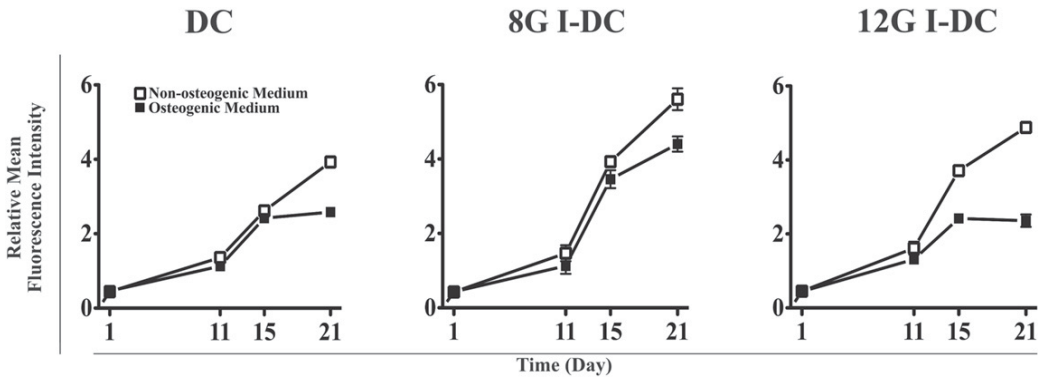

Figure 6. Seeded MSC metabolic activity. AlamarBlue™ metabolic activity analysis of seeded MSCs for up to day 21 of culture in nonosteogenic and osteogenic media. Error bars indicate standard deviations.

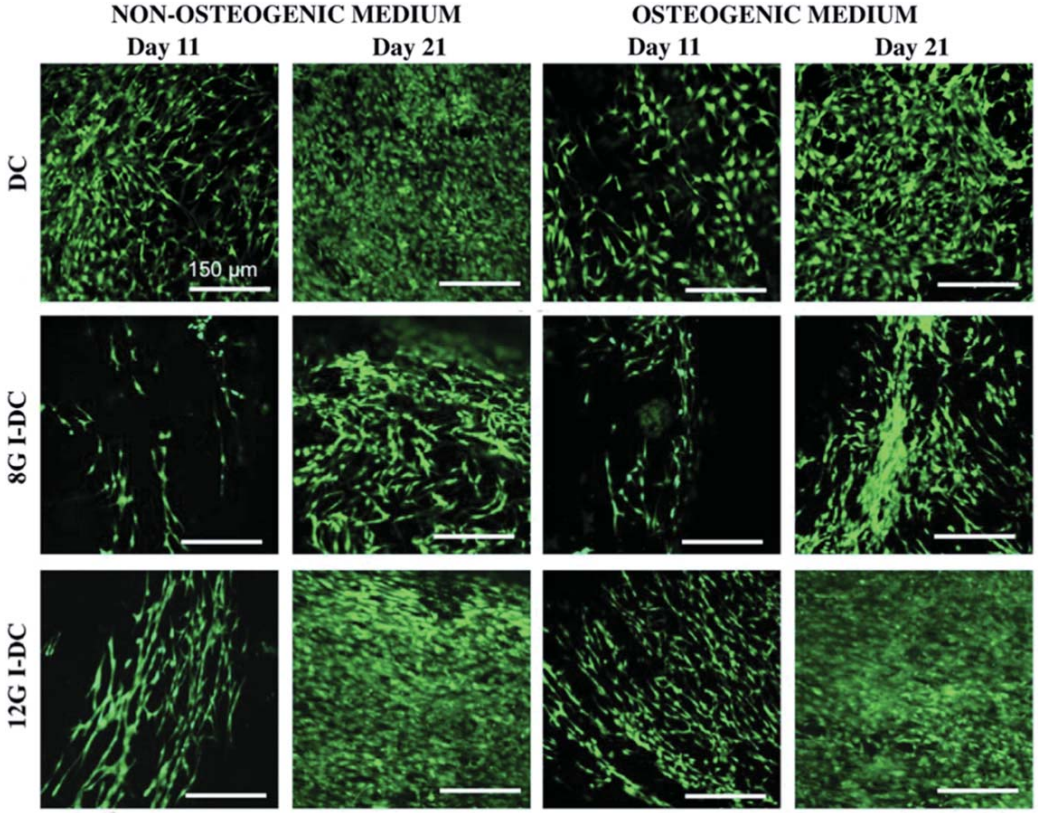

Figure 7. MSC viability and morphology. CLSM images of MSC seeded DC and 8G and 12G I-DC gels at days 11 and 21 of culture in nonosteogenic and osteogenic media (scale bar = 150 μm).

study, it was previously demonstrated that the extent of gel contraction was dependent on CFD and correlated with cell proliferation rates [17, 32]. Future studies will focus on investigating seeded cell-mediated matrix contraction in I-DC gels as a function of CFD and extent of alignment.

q-PCR analysis at days 11 and 21 assessed the expressions of *Alp*, *Runx*2/*Cbfa*1, and *Ocn*/*Bglap* as indicators of MSC osteoblastic differentiation [37] (figure 8). The data revealed that while the MSCs seeded in all gels differentiated into osteoblast-like cells when cultured osteogenic medium, there appeared to be no statistical difference ($p > 0.05$) in differentiation between 8G I-DC and DC gels. However, there was a greater extent of MSC osteoblastic differentiation in the 12G I-DC gels, which by day 11, demonstrated significantly ($p < 0.05$) higher expressions in all three gene transcripts, and at day 21, displayed significantly ($p < 0.05$) higher expression of *Ocn*/*Bglap*, a late marker for differentiation [39].

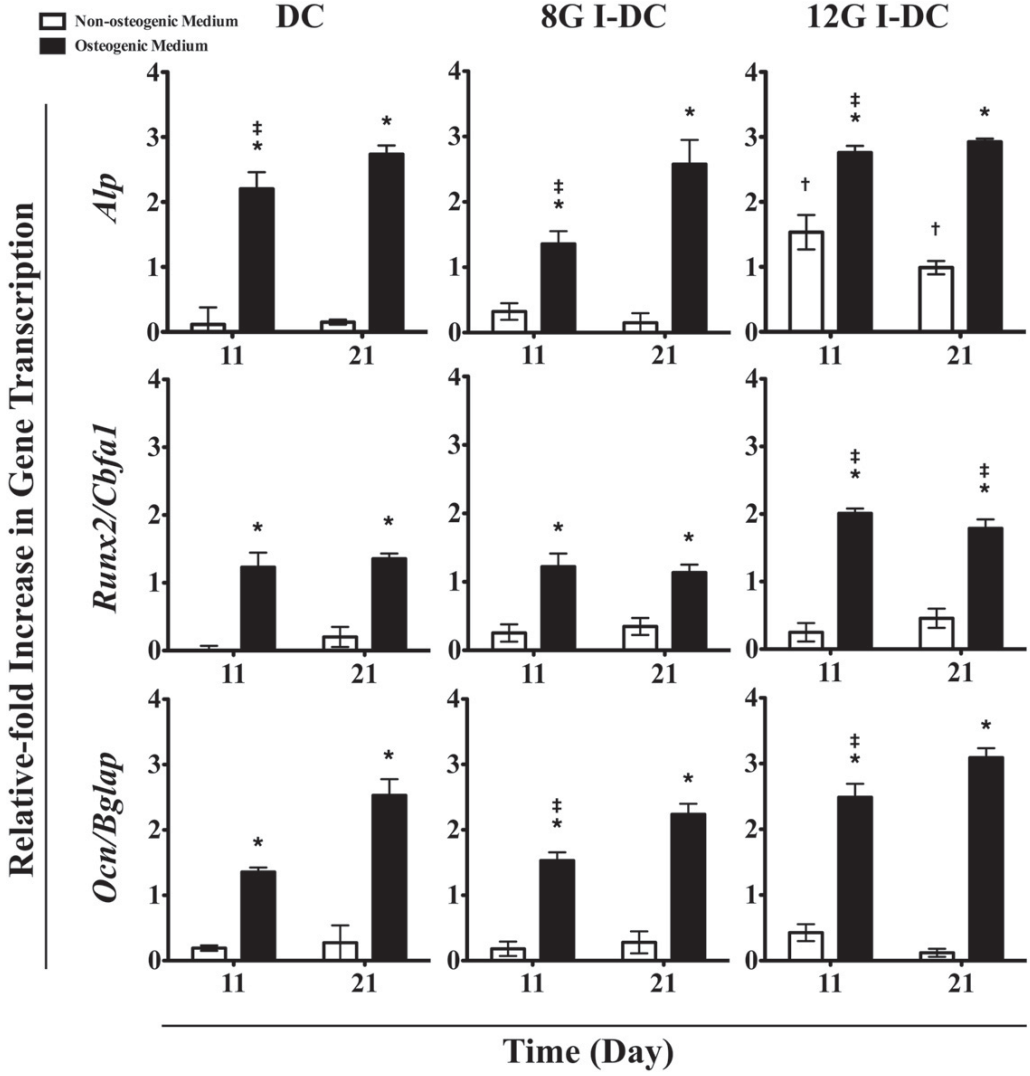

Figure 8. MSC osteogenic differentiation. q-PCR detection levels of *Alp*, *Runx*2, and *Ocn* of seeded MSCs for up to day 21 of culture in nonosteogenic and osteogenic media. * indicates significantly different expression levels in gels cultured in osteogenic and nonosteogenic media. † indicates that *Alp* expression in nonosteogenic 12G I-DC gels is significantly greater than the expression levels in DC and 8G I-DC gels. ‡ indicates expression levels of transcripts that are significantly greater than their comparable counterparts in other gels.

Expression of *Alp* in the 12G I-DC gel, cultured in nonosteogenic medium, was even significantly ($p < 0.05$) higher than that in 8G I-DC gels at day 11 in osteogenic medium. This relatively accelerated osteoblastic differentiation in 12G I-DC gels may be attributed to the combination of increased fibrillar alignment and physiologically relevant CFD, which enabled seeded cells to more rapidly differentiate as less matrix remodeling is necessary prior to the onset of differentiation [37]. While matrix stiffness modulation of MSC differentiation is known [40], it has been shown that MSCs seeded on aligned collagen nanofibers were more likely to differentiate when compared to those seeded on random fibrils [41]. The results of this study indicate that the 12G I-DC gel supported MSC osteoblastic differentiation by providing a 3D native tissue-equivalent environment.

4. Conclusions

The uniquely assembled GAE system provides a technique to rapidly and simply generate anisotropic, I-DC gels with highly defined microstructural, permeability, and mechanical properties. The ability to not only support homogenous cell seeding, but also to direct and accelerate their differentiation, creates numerous opportunities in regenerative medicine as well as drug and cell delivery.

Acknowledgments

Funding of CIHR, NSERC, CFI, Quebec MESRST (MDEIE), and McGill University Faculty of Engineering Gerald Hatch Faculty Fellowship are gratefully

acknowledged. The authors acknowledge Imaging and Molecular Biology Platform center (Pharmacology and Therapeutics Department, McGill University, Montreal) and thank Dr Wolfgang Reintsch for his technical assistance in NLSM imaging. The authors also acknowledge Dr Naser Muja for his technical assistance in recording the supplemental video.

References

[1] Langer R and Vacanti J P 1993 Tissue engineering *Science* **260** 920–6
[2] Slaughter B V, Khurshid S S, Fisher O Z, Khademhosseini A and Peppas N A 2009 Hydrogels in regenerative medicine *Adv. Mater.* **21** 3307–29
[3] Gross J and Kirk D 1958 The heat precipitation of collagen from neutral salt solutions: some rate-regulating factors *J. Biol. Chem.* **233** 355–60
[4] Bell E, Ivarsson B and Merrill C 1979 Production of a tissue-like structure by contraction of collagen lattices by human fibroblasts of different proliferative potential *in vitro Proc. Natl Acad. Sci. USA* **76** 1274–8
[5] Guidry C and Grinnell F 1987 Heparin modulates the organization of hydrated collagen gels and inhibits gel contraction by fibroblasts *J. Cell Biol.* **104** 1097–103
[6] Ruszczak Z and Friess W 2003 Collagen as a carrier for on-site delivery of antibacterial drugs *Adv. Drug Deliv. Rev.* **55** 1679–98
[7] Lai E S, Anderson C M and Fuller G G 2011 Designing a tubular matrix of oriented collagen fibrils for tissue engineering *Acta Biomater.* **7** 2448–56
[8] Fallas J A, O'Leary L E and Hartgerink J D 2010 Synthetic collagen mimics: self-assembly of homotrimers, heterotrimers and higher order structures *Chem. Soc. Rev.* **39** 3510–27
[9] Amini A A and Nair L S 2012 Injectable hydrogels for bone and cartilage repair *Biomed. Mater.* **7** 024105
[10] Knight D P, Nash L, Hu X W, Haffegee J and Ho M W 1998 *In vitro* formation by reverse dialysis of collagen gels containing highly oriented arrays of fibrils *J. Biomed. Mater. Res.* **41** 185–91
[11] Bessea L, Coulomb B, Lebreton-Decoster C and Giraud-Guille M M 2002 Production of ordered collagen matrices for three-dimensional cell culture *Biomaterials* **23** 27–36
[12] Mosser G, Anglo A, Helary C, Bouligand Y and Giraud-Guille M M 2006 Dense tissue-like collagen matrices formed in cell-free conditions *Matrix Biol.* **25** 3–13
[13] Brown R A, Wiseman M, Chuo C B, Cheema U and Nazhat S N 2005 Ultrarapid engineering of biomimetic materials and tissues: fabrication of nano- and microstructures by plastic compression *Adv. Funct. Mater.* **15** 1762–70
[14] Wang Y, Silvent J, Robin M, Babonneau F, Meddahi-Pellé A, Nassif N and Guille M M G 2011 Controlled collagen assembly to build dense tissue-like materials for tissue engineering *Soft Matter* **7** 9659–64
[15] Buxton P G, Bitar M, Gellynck K, Parkar M, Brown R A, Young A M, Knowles J C and Nazhat S N 2008 Dense collagen matrix accelerates osteogenic differentiation and rescues the apoptotic response to MMP inhibition *Bone* **43** 377–85
[16] Pedraza C E, Marelli B, Chicatun F, McKee M D and Nazhat S N 2010 An *in vitro* assessment of a cell-containing collagenous extracellular matrix-like scaffold for bone tissue engineering *J. Tissue Eng.* **16** 781–93
[17] Serpooshan V, Julien M, Nguyen O, Wang H, Li A, Muja N, Henderson J E and Nazhat S N 2010 Reduced hydraulic permeability of three-dimensional collagen scaffolds attenuates gel contraction and promotes the growth and differentiation of mesenchymal stem cells *Acta Biomater.* **6** 3978–87
[18] Coyac B R, Chicatun F, Hoac B, Nelea V, Chaussain C, Nazhat S N and McKee M D 2013 Mineralization of dense collagen hydrogel scaffolds by human pulp cells *J. Dent. Res.* **92** 648–54
[19] Marelli B, Ghezzi C, James-Bhasin M and Nazhat S 2015 Fabrication of injectable, cellular, anisotropic collagen tissue equivalents with modular fibrillar densities *Biomaterials* **37** 183–93
[20] Ghezzi C E, Marelli B, Muja N and Nazhat S N 2012 Immediate production of a tubular dense collagen construct with bioinspired mechanical properties *Acta Biomater.* **8** 1813–25
[21] Frank J, Balena R, Masarachia P, Seedor J G and Cartwright M 1993 The effects of three different demineralization agents on osteopontin localization in adult rat bone using immunohistochemistry *J. Histochem. Cytochem.* **99** 295–301
[22] Schindelin J *et al* 2012 Fiji: an open-source platform for biological-image analysis *Nat. Methods* **9** 678–82
[23] Al-Nasiry S, Geusens N, Hassens M, Luyten C and Pijnenborg R 2006 The use of Alamar blue assay for quantitative analysis of viability, migration and invasion of choriocarcinoma cells *Hum. Reprod.* **22** 1304–9
[24] Abou Neel E A, Cheema U, Knowles J C, Brown R A and Nazhat S N 2006 Use of multiple unconfined compression for control of collagen gel scaffold density and mechanical properties *Soft Matter* **2** 986–92
[25] Dalle Carbonare L and Giannini S 2004 Bone microarchitecture as an important determinant of bone strength *J. Endrocrinol. Invest.* **27** 99–105
[26] Evans F G and Vincentelli R 1969 Relation of collagen fiber orientation to some mechanical properties of human cortical bone *Int. J. Biomech.* **2** 63–71
[27] Kafantari H, Kounadi E, Fatouros M, Milonakis M and Tzaphlidou M 2000 Structural alterations in rat skin and bone collagen fibrils induced by ovariectomy *Bone* **26** 349–53
[28] Dahoun A, Aboulfaraj M, G'Sell C, Molinari A and Canova G R 1995 Plastic behavior and deformation textures of poly (etherether ketone) under uniaxial tension and simple shear *Polym. Eng. Sci.* **35** 317–30
[29] Fratzl P 2008 *Collagen: Structure and Mechanics* (New York: Springer)
[30] Swartz M A and Fleury M E 2007 Interstitial flow and its effects in soft tissues *Annu. Rev. Biophys. Eng.* **9** 229–56
[31] Jiang H and Grinnell F 2005 Cell–matrix entanglement and mechanical anchorage of fibroblasts in three-dimensional collagen matrices *Mol. Biol. Cell* **16** 5070–6
[32] Serpooshan V, Muja N, Marelli B and Nazhat S N 2011 Fibroblast contractility and growth in plastic compressed collagen gel scaffolds with microstructures correlated with hydraulic permeability *J. Biomed. Mater. Res. Part* A **96** 609–20
[33] Nirmalanandhan V S, Levy M S, Huth A J and Butler D L 2006 Effects of cell seeding density and collagen concentration on contraction kinetics of mesenchymal stem cell-seeded collagen constructs *J. Tissue Eng.* **12** 1865–72
[34] Censi R, Di Martino P, Vermonden T and Hennink W E 2012 Hydrogels for protein delivery in tissue engineering *J. Control. Release* **161** 680–92
[35] Jaiswal N, Haynesworth S E, Caplan A I and Bruder S P 1997 Osteogenic differentiation of purified, culture-expanded human mesenchymal stem cells *in vitro J. Cell. Biochem.* **64** 295–312
[36] Rampersad S N 2012 Multiple applications of Alamar Blue as an indicator of metabolic function and cellular health in cell viability bioassays *Sensors (Basel, Switzerland)* **12** 12347–60
[37] Bitar M, Brown R A, Salih V, Kidane A G, Knowles J C and Nazhat S N 2008 Effect of cell density on osteoblastic differentiation and matrix degradation of biomimetic dense collagen scaffolds *Biomacromolecules* **9** 129–35
[38] Marelli B, Ghezzi C E, Alessandrino A, Freddi G and Nazhat S N 2014 Anionic fibroin-derived polypeptides accelerate MSC osteoblastic differentiation in a three-dimensional osteoid-like dense collagen niche *J. Mater. Chem.* B **2** 5339–43
[39] Bharadwaj S, Naidu A G, Betageri G V, Prasadarao N V and Naidu A S 2009 Milk ribonuclease-enriched lactoferrin

induces positive effects on bone turnover markers in postmenopausal women *Osteoporis. Int.* **20** 1603–11
[40] Engler A J, Sen S, Sweeney H L and Discher D E 2006 Matrix elasticity directs stem cell lineage specification *Cell* **126** 677
[41] Subramony S D, Dargis B R, Castillo M, Azeloglu E U, Tracey M S, Su A and Lu H H 2013 The guidance of stem cell differentiation by substrate alignment and mechanical stimulation *Biomaterials* **34** 1942–53